5-2017

Infrared Study of Recluse Spider Silk

Stephanie Wang
College of William and Mary

Infrared Study of Recluse Spider Silk

A thesis submitted in partial fulfillment of the requirement
for the degree of Bachelor of Science in Physics from
The College of William and Mary

by

Stephanie Wang

Accepted for _____
(Honors or no-Honors)

_____
M Mumtaz Qazilbash, Physics, Director

_____
Gina Hoatson, Physics

_____
Hannes Schniepp, Applied Science

Williamsburg, VA
April 28, 2017

Table of Contents

Abstract

We want to gain insight into the composition and structure of spider silk to discover the origin of its extremely high mechanical properties. We are especially interested in the organization of the crystalline ß-sheets that are expected to contribute to the high strength of the silk from the recluse spider, *Loxosceles laeta*. The recluse spider produces a thin, ribbon-like silk, which has a unique geometry amongst arachnids. We measure the silk's optical properties, particularly the infrared-active vibrations. Broadband infrared transmission spectra were collected in the spectral range between 600 cm^{-1} and 4000 cm^{-1}, with light polarized parallel and perpendicular to the long axis of the silk. The infrared vibrational modes are fit with Lorentzian and Voigt functions. The vibrational modes are assigned to specific structures and electronic bonds in the silk. We find that at least one-fourth of the recluse spider silk consists of crystalline ß-sheets.

I. INTRODUCTION

Silk from spiders and silkworms exhibits remarkable mechanical properties. For example, it is incredibly strong but lightweight and exceedingly tough at the same time[1]. Its exceptional strength exceeds that of steel[2]. It is among Nature's toughest materials, with the capacity for increased toughness when spun into microloops[3]. Because of its extraordinary mechanical properties, suitably processed silk is a proposed material for technical textiles, bio-integrated electronics, and medical applications[4–6].

The two components that determine the properties of silk are the molecular design of the protein components and the hierarchical organization of structural elements[7]. Silk is comprised of flexible, amorphous chains that are reinforced by smaller, stiff crystalline structures[8]. This arrangement is crucial in giving silk its high strength. The amorphous chains are made of

glycine-rich spiral regions of spidroin, the main protein in spider silk. It is the organization of the ß-sheets in the crystalline structures that contributes to the high strength of the silk[8–12].

Here, we study silk from the recluse spider *Loxosceles laeta*, which differs from the silk of other spiders in a few significant ways. The recluse spider produces a silk that is ribbon-like with a rectangular cross-section, while most spider silks have a circular cross section[1,13]. This unique geometry is seen in Figure 1. The recluse spider silk is only 40-80 nanometers thick with an aspect ratio of about 100:1. Its cross sectional area is much smaller than silk from other spiders[1,13]. Despite being thinner and lighter than most other spider silks, the silk of the recluse spider is amongst the strongest in the arachnid community. The flat, ribbon-like geometry makes it very sticky, and it adheres easily to most surfaces that it touches[1]. Additionally, the silk of the recluse spider exhibits high stiffness compared to silk from other spiders that have a circular cross section[1].

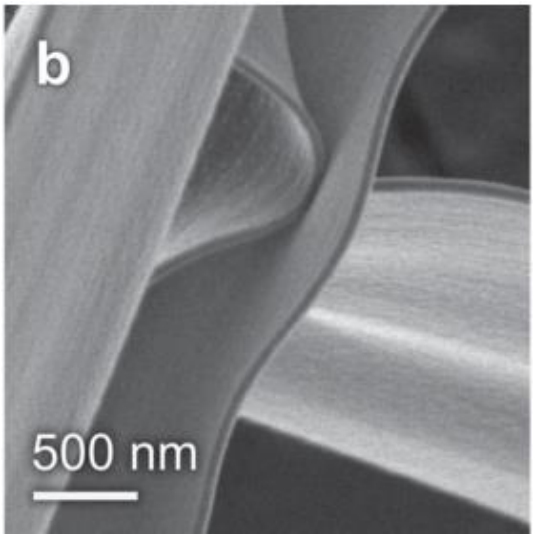

Figure 1: SEM image of recluse spider silk, showing its flat, ribbon-like nature[1].

Previously, various optical techniques have been applied to spider silk to study its structure and its composition, such as Fourier Transform Infrared (FTIR) Spectroscopy and Raman spectroscopy[8,14–17]. In this work, we characterize the macroscopic optical properties with FTIR spectroscopy using polarized light, particularly the infrared active vibrations of the components of recluse spider silk. The vibrational modes are fingerprints of the structure and chemical composition of the material. Previous studies have found that the surface of the recluse spider silk has a fibrillar texture, similar to the skin of other cylindrically shaped spider silks that show skin-core morphology[1]. These fibrils run along the long axis of the silk further motivating a study using light polarized parallel and perpendicular to the long axis of the silk strands.

II. EXPERIMENTAL METHODS

A. Sample Preparations

Silk samples are taken from three different recluse spiders, two female and one male. These samples were provided by the Schniepp group in the Applied Science Department at William & Mary. The silk strands are 40-80 nm thick, and about 10 μm wide[1]. The silk strand is wrapped around a 1.3 mm diameter aperture in a rectangular metal piece. A photograph of this setup can be seen in Figure 2. One sample from a female spider contains 300 turns of silk, while the other two samples each contain 100 turns of silk. In this work, we will primarily discuss data from the sample with 100 turns of female spider silk. Note that the infrared-active vibrational modes for all samples occur at identical frequencies.

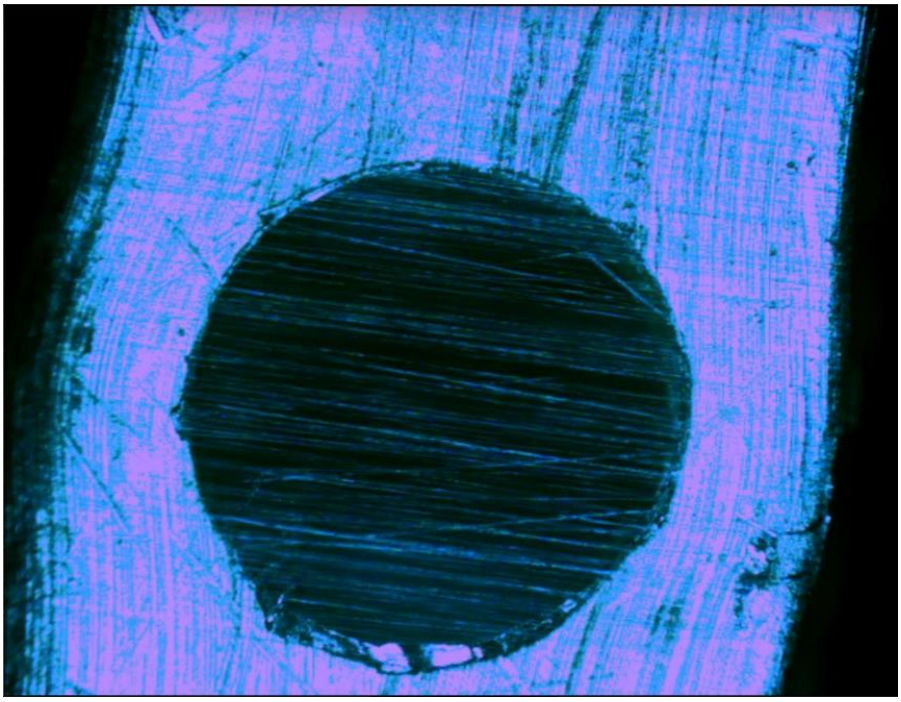

Figure 2: 100 turn silk sample on a holder for infrared transmission measurements.

B. Infrared Measurements

Broadband infrared transmission spectra were collected with a Bruker 80v vacuum spectrometer in the spectral range between 600 cm^{-1} and 4000 cm^{-1}, with a spectral resolution of 4 cm^{-1}. A polarizer consisting of a wire grid on KRS-5 substrate was mounted to an electronically controlled step motor rotation stage inside the vacuum chamber of the spectrometer to obtain data for light polarized parallel and perpendicular to the silk strands. A liquid nitrogen cooled mercury-cadmium-telluride (MCT) photoconductor was used for infrared detection. The infrared transmission data through the spider silk sample was normalized relative to the transmission through an aperture of the same diameter as that used for the silk. The translation between the silk specimen and the reference aperture is implemented using a very accurate motorized stage in the sample compartment of the spectrometer. The infrared experiments were performed in Professor Qazilbash's lab in the Physics Department at William & Mary.

III. **RESULTS AND DISCUSSION**

A. Background Removal

To investigate the anisotropy of the silk, we took measurements in two orientations: with the light polarized parallel and perpendicular to the long (spinning) axis of the silk. The infrared transmission spectra show a frequency dependent background. This background likely occurs as a result of frequency dependent diffraction, reflectance and scattering due to the geometry of the specimen of spider silk fibers used for transmission measurements. There is an uncertainty of about 1% in the absolute value of the transmission which may be due to slight misalignment of the reference (open hole) and the silk specimen. We are able to remove this background by excluding the spectral range of infrared vibrational modes, and using a polynomial to fit the remaining featureless spectrum which is mainly attributed to transmission background. We then subtract this polynomial fit from the raw transmission data to obtain a background-free transmission spectrum. A graph of this process is shown in Figure 3.

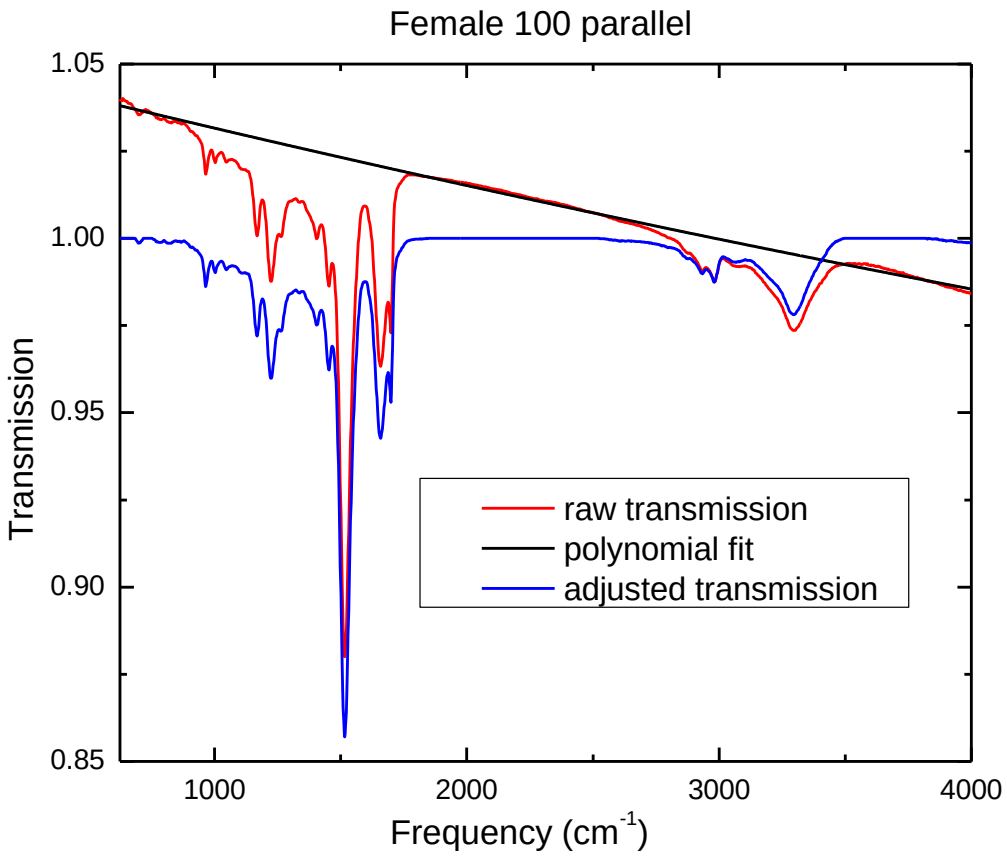

Figure 3: Transmission spectrum for silk from female spider with 100 turns. Light is polarized parallel to the long axis. We can see the raw transmission with the frequency dependent background, the polynomial used to fit the background, and the adjusted transmission that is background free. An identical process is used to remove the background for all transmission measurements.

B. Modelling the Data

To analyze the data, we use a combination of Lorentz and Gauss-Lorentz oscillators to fit the transmission spectra, and these fitting parameters are characteristic of the particular type of proteins present, as well as their orientation. The Lorentz oscillator parameters are characteristic of the particular type of proteins present, as well as their orientation. The Lorentz oscillator represents the interactions of the atoms with the time-varying electric field. The Lorentz model

is analogous to a damped harmonic oscillator[18,19]. In this model, we view the atoms as masses connected with springs that obey Hooke's law, which can be seen in Figure 4.

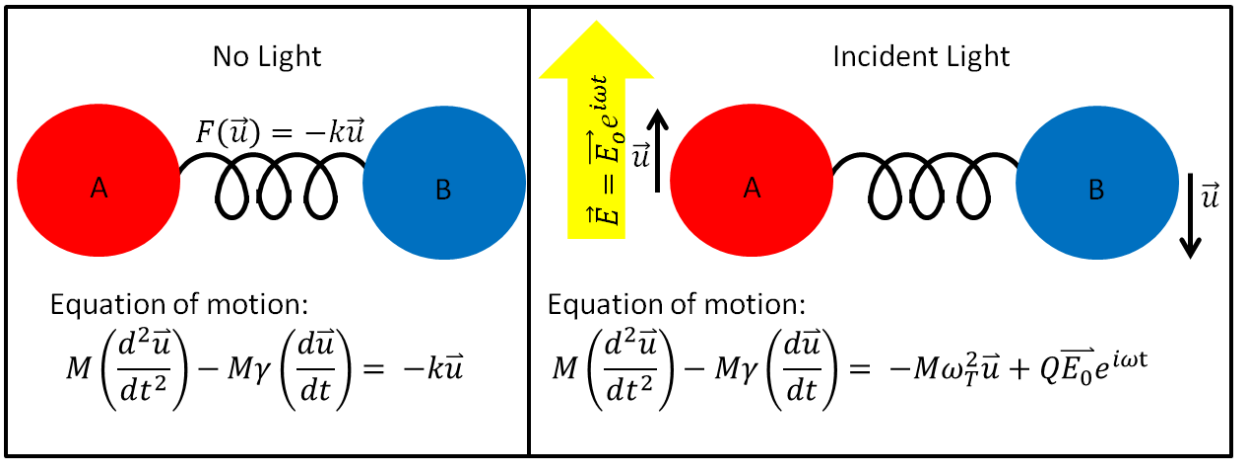

Figure 4: An example of a polar covalent molecule, where A and B are covalently bonded atoms.

The driving force acting on this spring model is the electric field interacting with a charged particle. When an oscillating electric field in a light ray is incident on this system, the system will go into harmonic motion, with an equation of motion

$$M\left(\frac{d^2\vec{u}}{dt^2}\right) - M\gamma\left(\frac{d\vec{u}}{dt}\right) = -M\omega_T^2\vec{u} + QE_0e^{i\omega t}\hat{e},$$

where M is the reduced mass, $\vec{u}$ is the displacement from the equilibrium position, γ is the damping factor, ω_T is the natural frequency of the oscillators, ω is the frequency of electric field, Q is the charge of the oscillators, E_0 is the amplitude of the electric field, and $\hat{e}$ is the direction of the polarization of the incident electric field.

We assume $\vec{u} = \vec{u}_o e^{i\omega t}$, where ω is the frequency of the oscillator. Recalling that $\vec{P} = NQ\vec{u}$, where $\vec{P}$ is the polarization field and N is the density of the oscillators, some algebra yields

$$\vec{P} = \frac{NQ^2}{M(\omega_T^2 - \omega^2 - i\omega\gamma)}\vec{E}\,.$$

Recall that the dielectric constant, $\varepsilon(\omega)$, is defined by the relation

$$\vec{D} = \varepsilon(\omega)\vec{E} = \vec{E} + 4\pi\vec{P}\,.$$

Substituting in the expression for the polarization field, we find that

$$\varepsilon(\omega)\vec{E} = \left(1 + \frac{4\pi NQ^2}{M(\omega_T^2 - \omega^2 - i\omega\gamma)}\right)\vec{E}\,.$$

The resulting dielectric constant is then

$$\varepsilon(\omega) = 1 + \frac{4\pi NQ^2}{M(\omega_T^2 - \omega^2 - i\omega\gamma)}\,.$$

However, it is worthwhile noting that we had assumed that the dielectric constant is zero outside of the region of interest. Since this is not necessarily the case, it is useful to make the correction:

$$\varepsilon(\omega) = \varepsilon_\infty + \frac{4\pi NQ^2}{M(\omega_T^2 - \omega^2 - i\omega\gamma)},$$

where ε_∞ is the dielectric constant at frequencies higher than the spectral range of infrared-active vibrations . This can also be rewritten as

$$\varepsilon(\omega) = \varepsilon_\infty + \frac{\varepsilon_0 - \varepsilon_\infty}{1 - {\omega^2}/{\omega_T^2} - i\,{\omega\gamma}/{\omega_T^2}}.$$

The index of refraction is given by $n = \varepsilon^{1/2}$. Note that the spider silk we are looking at is anisotropic, but these equations are still applicable because we study the silk with polarized light. The dielectric function describes how the material responds to electromagnetic radiation.

Due to the complicated geometry of the specimen, we cannot reliably obtain the absolute value of the dielectric function from the transmission measurements. However, the relative amplitude of the Lorentz oscillators, and the absolute values of their center frequencies (ω_T) and their linewidths (γ) provide a wealth of information.

Spectral lines are, in theory, infinitely sharp. However, there are various effects present that contribute to the broadening of the spectral line. For instance, there is a natural broadening that occurs due to the uncertainty principle[20]. A shorter lifetime of an excited state will have a larger energy uncertainty and a broad emission profile. There is an additional effect due to thermal motion, called the Doppler broadening. This does not affect all molecules in the same manner and results in a Gaussian distribution[20]. Another prominent factor is the proximity broadening. This states that all molecules that are nearby affect each other, which in turn affects the line width and position. Each of these broadening mechanisms affects the observed line profile. Thus, we are able to fit our spectrum with a convolution of Gaussians and Lorenztians, using Voigt functions. Simply, we use Voigt functions to fit the data since they convolve a natural Lorentzian with a Gaussian instrument broadening[21]. Additionally, while it is true that that simple molecules exhibit an infrared spectrum that is purely Lorentzian in shape, complex molecules, such as proteins, do not necessarily follow this rule[22].

We use the following parameters to produce a Gaussian fit[23]:

$$\varepsilon_{n_{Gaussian}} = \varepsilon_{n_1} + i\varepsilon_{n_2}, \text{ where}$$

$$\varepsilon_{n_2} = A'e^{-\left(\frac{E-E_n}{\sigma}\right)^2} - A'e^{-\left(\frac{E+E_n}{\sigma}\right)^2},$$

$$\sigma = \frac{Br_n}{2\sqrt{ln2}}, \text{ and}$$

$$\varepsilon_{n_1} = \frac{2}{\pi} P \int_0^\infty \frac{\xi \epsilon_{n_2}(\xi)}{\xi^2 - E^2}\, d\xi.$$

Further, we convolve a Gaussian with a Lorentzian to produce a Voigt function, which takes the following form for the nth oscillator[23] :

$\epsilon_n(E) = iA_n\left[\int_0^\infty e^{i\left(E - E_n + i\gamma_n(s)\right)s}\, ds - \int_0^\infty e^{i\left(E + E_n + i\gamma_n(s)\right)s}\, ds\right] / \left[\int_0^\infty e^{-s\gamma_n(s)}\, ds\right]$, where

$$\gamma_n(s) = \Gamma_n + 2\sigma_n^2 s$$

We are able to vary the broadening between Lorentzian and Gaussian using the following equations:

$$Br_n^2 = B_{Lorentz_n} + B_{Gaussian_n}^2$$

$$\Gamma_n = \frac{1}{2} B_{Lorentz_n}$$

$$\sigma_n = \frac{1}{4\sqrt{ln4}} B_{Gaussian_n}$$

All infrared transmission spectra are fitted using WVASE software from Woollam Inc.

C. Absorption Data

Note that we also converted the transmission spectrum to an absorption spectrum by using the following formula:

$$A = -\log\left(\frac{I}{I_0}\right),$$

where I_0 is the intensity of the beam transmitted through the reference aperture, and I is the intensity of the beam transmitted through the silk specimen. This formula stems from the Beer-Lambert Law. The absorption spectra are shown in Figure 5.

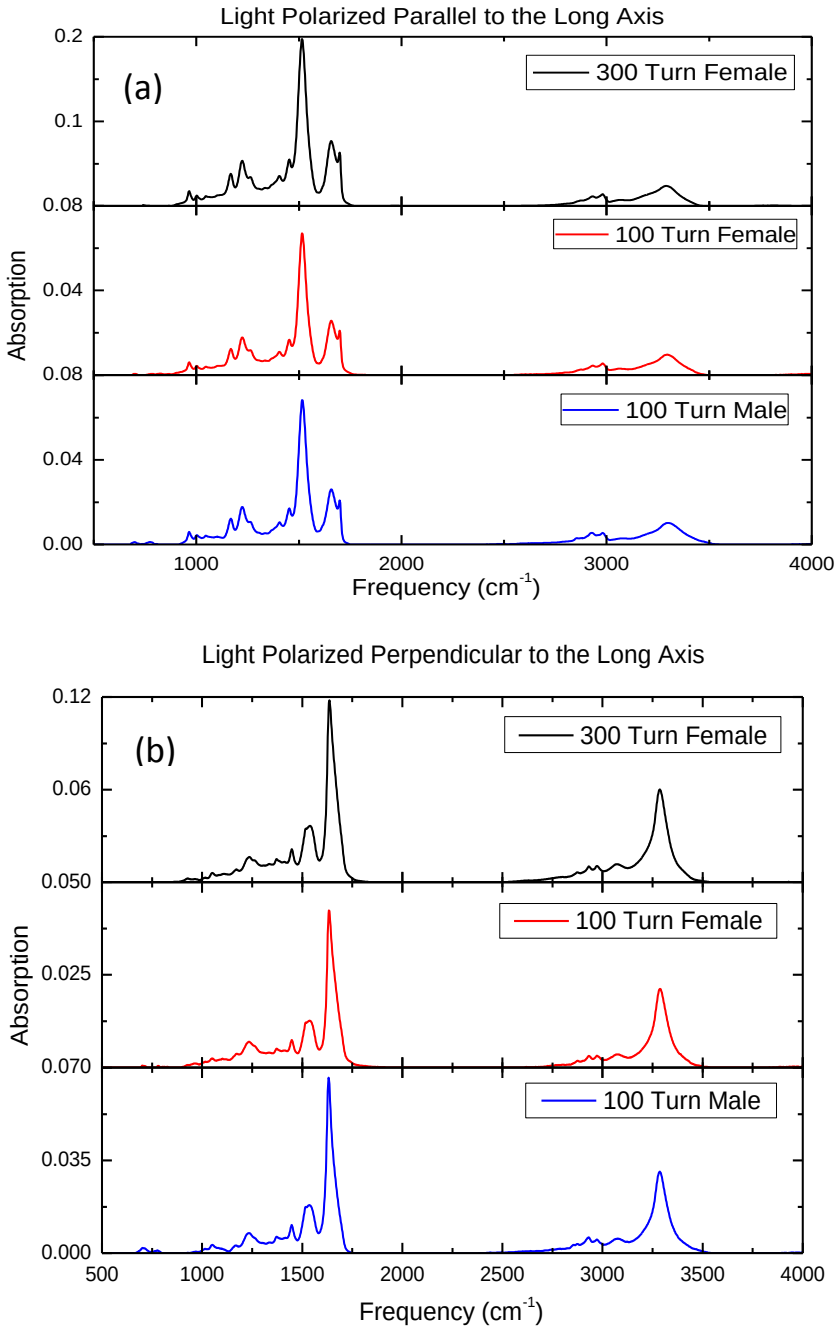

Figure 5: Infrared absorption data for all samples. (a) Data taken with light polarized parallel to the long axis of the silk. (b) Data taken with light polarized perpendicular to the long axis of the silk.

D. Infrared Active Vibrational Modes

In table 1 and table 2 we can see that the most prominent line assignments of the vibrational modes include ß-sheet with polyalanine domains and amides. ß-sheets are one of the main structures we see in the silk, shown in Figure 6. They are the crystalline regions of the silk and are often poly-Ala structures with alanine residues[24]. ß-sheets are very distinct and contain a hydrogen face as well as a methyl and methanolic group comprising another face[25]. They exist on the order of a few nanometers, and consist of a dense network of hydrogen bonds[26–28].A study conducted using electron diffraction on spider dragline silk found the space group of ß-sheets to be $P2_1$[29]. This means that the crystal system of the ß-sheet is monoclinic with a two-fold axis of rotational symmetry but is not centrosymmetric.

Table 1: Infrared vibrational modes in the recluse spider silk data for polarization parallel to the long axis of the silk. Molecular assignments are based on values from the literature for similar organic compounds.

Center Frequency (cm^{-1}) of infrared modes of recluse spider silk	**Molecular Assignment**	**Frequency from literature**	**Normalized Amplitude**	**Broadening (cm^{-1})**
700.58	CN tor, NH opb, NH—O opb	704[30]	0.0202	20
782.37	α-helical Poly(L-alanine) CO opb, $NC^{\alpha}C$ def	774[31]	0.0122	15.74
821.13			0.0136	21.813
905.31	Poly L-ala(CH_3 rock, CN str., CNC_{α} def., C_{α}-C_{β} str., C==O str.)	906[32]	0.0123	14.449
930.09	CN str., CH_3 rock 2, NC^{α} str., $C^{\alpha}C^{\beta}$ str.	926[30]	0.0197	30.904
965.71	β-PAla (CH_3 rock, N-C_{α} stretch)	963[17]	0.1357	21.706
1002.9	$(AlaGly)_n$ CH_3 chain	1000[17]	0.0702	25.02
1049.3	PPro I (C_{α}-C_{β}-C_{γ} stretch), other amino acids	1049[17]	0.0613	48.45
1106	CH_3 rock, C_{α}-C_{β} str.	1106[33]	0.0599	60
1167.6	β -PAla (H_{α} bend, CH_3 sym. b., C_{α}-C_{β} str.)	1167[17]	0.2193	31
1221.5	Amide III β-Sheet	1224[15]	0.2054	32.6
1231	Amide III Random Coil	1235[15]	0.1232	66.6
1265.4	Amide III α-helix	1265[15]	0.1392	37
1306.7	β -PAla (CN stretch, H_{α} bend)	1306[32]	0.0473	39.167
1336.5	CH_3 sym. bend, H_{α} bend, NH ipb	1332[30]	0.0557	40
1365	H_{α} bend, NH ipb, CH_3 sym. bend	1359[30]	0.0491	28.738
1383.2	CH_3 sym. bend	1378-1390[33]	0.0393	25.476
1405.7	Poly L-ala(H_{α} bend, ,	1405[34]	0.1211	36.567

	CH_3 sym. b., NC_α str.)			
1450.6	β -PAla (CH_3 asym. Bend)	1454[17]	0.1706	24.351
1513	Amide II	1521[17]	1.0000	37.69
1532			0.2882	36
1643.4	Amide I C=O stretching[35], Random coil	1648[35]	0.0801	27.268
1660	Amide I C=O stretching[35], 3_{10} Helix	1663[35]	0.3098	45
1683	Amide I C=O stretching[35], β sheet	1683[35]	0.0452	41
1699.2	Amide I C=O stretching[35], β sheet	1697[17]	0.1810	12.5
2875	β -PAla (C_α-H_α stretch)	2874[32]	0.0118	140
2933.1	Crystalline Polyglycine I ($C^\alpha H$ asym str)	2929[36]	0.0226	50
2963			0.0035	36
2980.8	β -PAla (CH_3 asymmetric stretch)	2980[32]	0.0285	32.412
3063.5	Amide B	3030-3100[37]	0.0139	98
3150			0.0049	80
3208			0.0196	110
3298	Amide A NH stretching	3300[35]	0.0644	112
3370			0.0080	112

Table 2: Infrared vibrational modes in the recluse spider silk data for polarization perpendicular to the long axis of the silk. Molecular assignments are based on values from the literature for similar organic compounds.

Center Frequency (cm^{-1}) of infrared modes of recluse spider silk	**Molecular Assignment**	**Frequency from literature**	**Normalized Amplitude**	**Broadening (cm^{-1})**
705	CN tor, NH opb, NH—O opb	704[30]	0.0370	18
780	β -PAla (CO ib, NC^{α} s, $C^{\alpha}C$ s, $NC^{\alpha}C$ d, CNC^{α} d, C^{β} B)	778[32]	0.0185	15
925	CN str., CH_3 rock 2, NC^{α} str., $C^{\alpha}C^{\beta}$ str.	926[30]	0.0157	13
962	β-PAla (CH_3 rock, N-C_{α} stretch)	963[17]	0.0399	50
1014	Skeletal stretching mode for PGI	1015[38]	0.0449	24
1051	β -PAla (C_{α}-C_{β} str., H_{α} bend)	1055[17]	0.0855	32
1097	CH_3 rock, C_{α}-C_{β} str.	1095[30]	0.0641	50
1120	NC str., C_{α}-C_{β} str.	1116[33]	0.0214	35
1170	β -PAla (C_{α}-C_{β} stretch, H_{α} bend, CH_3 symmetric angle bend)	1167[32]	0.0826	35
1231	Amide III Random coil	1235[15]	0.2521	66.6
1267.5	Amide III α-helix	1265[15]	0.0712	39.429
1304.8	β -PAla (CN stretch, H_{α} bend)	1306[32]	0.0558	50
1337.2	CH_2 wagging mode	1338[36]	0.0715	45
1370.8	β -PAla (CH_3 symmetric angle bend, H_{α} bend)	1372[32]	0.0866	24
1387	β -PAla (CH_3 sb, H^{α} b, $C^{\alpha}C^{\beta}$ str.)	1386[32]	0.0356	28
1410.8	CH_2 wagging mode	1409[38]	0.0905	50
1448	β -PAla (CH_3 asymmetrical angle	1444[32]	0.1781	23.943

	bend)			
1517	Amide II CN stretch, NH bending[35]	1520[38]	0.2635	40.645
1545	Amide II CN stretch, NH bending	1542[17]	0.2635	45
1633	Amide I C=O stretching[35]	1620-1640[35]	1.0000	22.5
1647	Amide I, Random Coil	1648[35]	0.2279	26
1663	Amide I, β -Turn	1665[35]	0.5271	55
2792			0.0071	127.46
2872	β -PAla (C_α-H_α stretch)	2874[32]	0.0171	40
2930	$C^\alpha H$ asym str	2929[36]	0.0399	37
2972	CH_3 asym str	2970[30]	0.0328	39.5
3073	Amide B	3030-3100[37]	0.0427	90
3234	Amide A NH stretching	3242[32]	0.0271	140
3289	Amide A NH stretching	3285[38]	0.3148	80

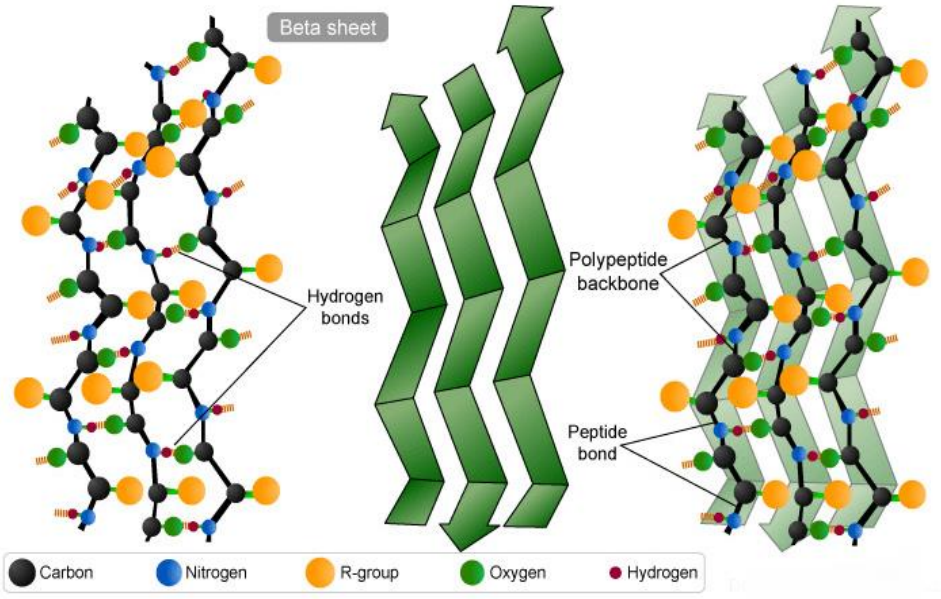

Figure 6: Structure of a ß-sheet.

An amide is an organic compound with a structure that includes an O=C—N group. They are amongst the characteristic bands that are regularly found in the infrared spectra of proteins and polypeptides, as they link amino acids. Amide I absorption is associated with stretching vibrations of C=O bonds, while Amide II absorption is associated with bending vibrations of the N—H bond[39]. Amide III is a broad band that is comprised of C—C stretching, C==O stretching, C—N stretching, and N—H bending[40]. All of these bonds are important in the hydrogen bonding responsible for the secondary structure of protein. It is important to note that the Amide I band is difficult to resolve because the amplitude is small compared to the intrinsic width of the band—one broad peak is observed instead of many well resolved peaks[39]. We note that another prominent amide, Amide A, occurs between 3270 and 3310 cm^{-1}, depending on the strength of the hydrogen bond[37]. Amide A comes from the NH stretching vibration, and is localized on the NH group[37]. The second component, Amide B, is weaker and occurs between 3030 and 3100 cm^{-1} [37].

The polarized infrared data suggests that the silk of the recluse spider is anisotropic because of differences between the spectra for polarizations parallel and perpendicular to the long axis of the silk. There are fewer vibrational modes apparent in the data obtained with polarization perpendicular to the long axis of the silk. Both polarizations show a large mode at ~1500-1600 cm^{-1} arising from the Amide II structure, which is comprised of the ß-sheet, α-helix, and random coil. Images of the α-helix and random coil are shown in figures 7 and 8. However, it is much stronger in the parallel polarization. The parallel polarization shows an additional large mode at ~1660 cm^{-1}. Also note that the N-H stretching Amide A mode at ~ 3300 cm^{-1} appears more strongly in the data obtained with polarization perpendicular to the long axis of the silk.

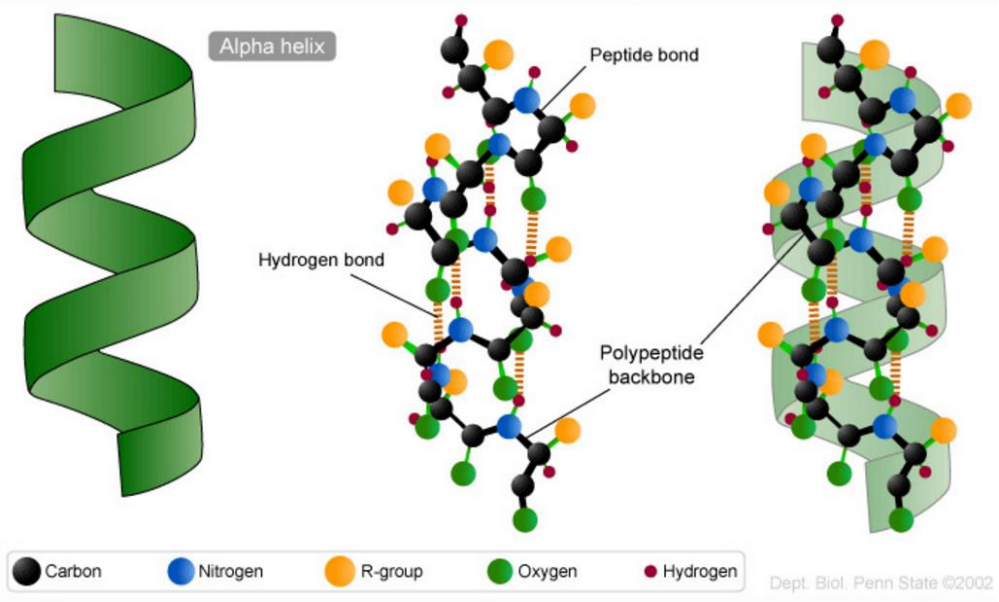

Figure 7: An α-helix is a form of secondary structure in proteins. This is helix shaped, and every backbone (N-H group) is hydrogen bonded to the (C=O group) backbone of the amino acid along the protein sequence. This is found in the Amide III region.

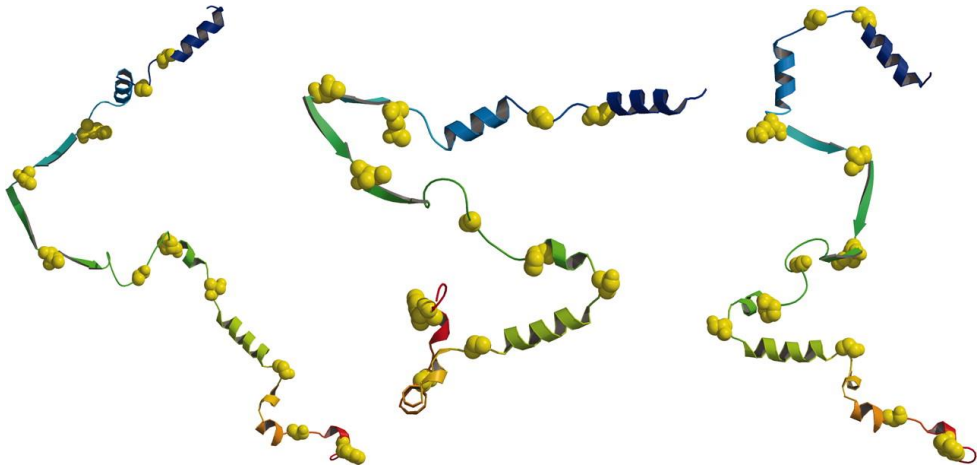

Figure 8: A random coil is a polymer structure where all the subunits (monomers) are oriented randomly. This is not in a specific shape. This is found in the Amide III region.

In both polarizations, the vibrational modes occur in two distinct groups, one from ~700 to 1700 cm^{-1}, and one from ~2800 to 3300 cm^{-1}. This stems from the vibrational frequency,

$\omega_T^2 = k/M$ relationship, where k is an effective spring constant that signifies the bond strength.. The modes at higher frequencies arise from vibrations of lighter elements, such as hydrogen. Moreover, they originate from stronger chemical bonds with higher effective spring constants and tend to be stretching modes.[40]. Conversely, modes at lower frequencies arise from heavier elements, such as carbon, nitrogen, and oxygen, and are more likely to be bending modes with lower effective spring constants [40].

E. ß-Sheet Calculations

In order to calculate the percentage of ß-sheets in the silk, we performed deconvolution on the amide III band, in the 1180- 1300 cm^{-1} region [15]. Analyzing the amide III region for band assignments has obvious benefits. It is easily resolved and has structured spectral contour[41]. The bands are better defined than other regions, such as the amide I[42], and can be used to study secondary structural contents.

We are able to quantitatively determine the beta-sheet content of the recluse spider silk by modeling the features from the amide III structure in the transmission data. We use Gauss-Lorentz functions to model the transmission data and assign the valleys in the data to infrared modes from α-helix, random coil, or ß-sheet, shown in Figure 9.

We first fit the Amide III band in the perpendicular polarization, and then use the same parameters to fit the parallel polarization. As the ß-sheet is strongly aligned along the long axis of the silk, we do not see a contribution from the ß-sheet in the data where light is polarized perpendicular to the spinning axis[14,17,43]. Based on the relative areas of the Gauss-Lorentz functions that describe the relevant modes in the transmission data, we obtain a 26% ß-sheet composition. This silk was also studied using Raman spectroscopy by our collaborator in the

Schniepp group. A similar deconvolution was performed on the Amide I band, which yielded a 26% ß-sheet composition. The agreement between these two measurements confirms the percentage of ß-sheets present in the silk are consistent.

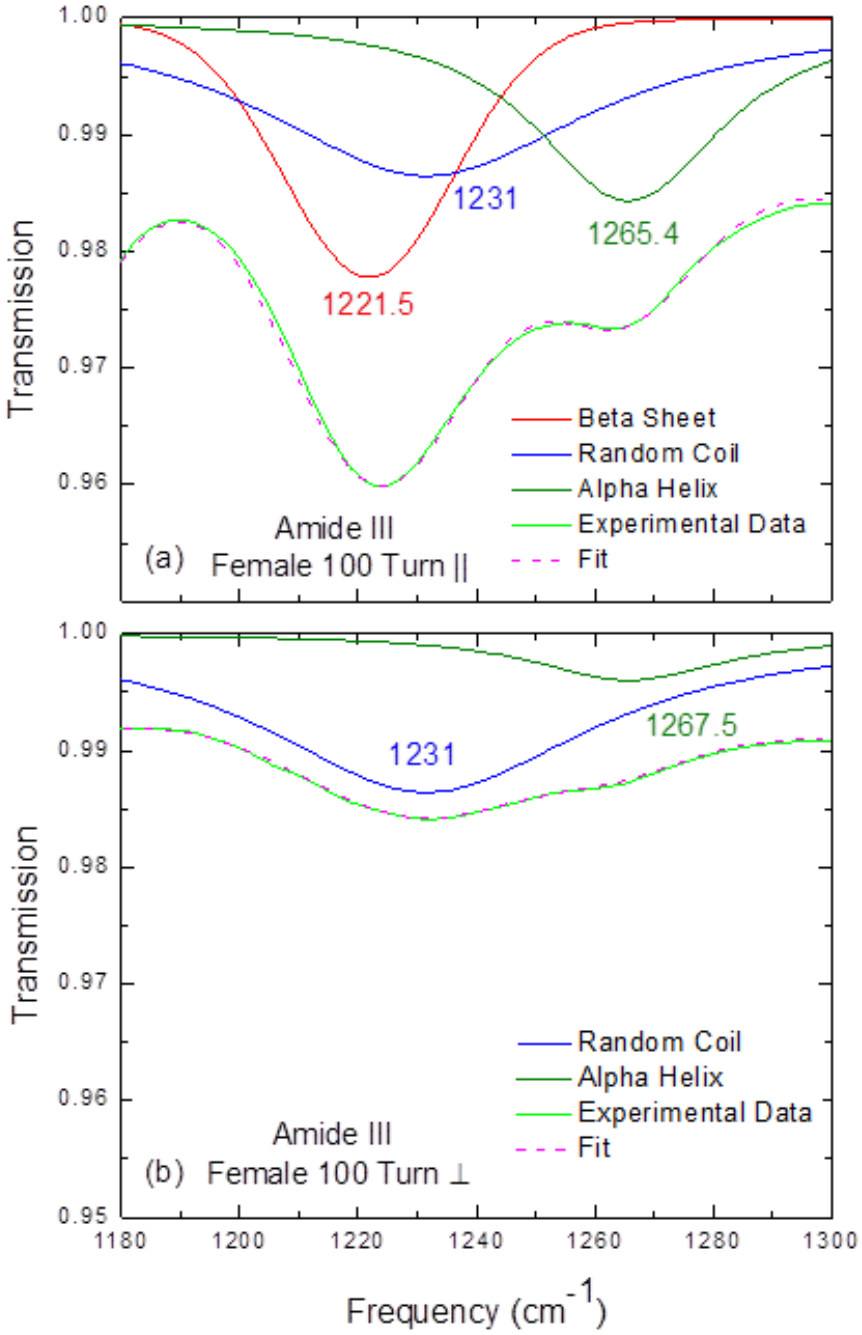

Figure 9: Deconvolution of the amide III region, 1180-1300 cm^{-1}. The fits as well as the experimental data are shown. Center frequencies of oscillators are labeled in the figure. (a) The parallel polarization, where light is polarized along the long axis of the silk. We can deconstruct this band into components arising from alpha helix, ß-sheet, and random coil. (b) The perpendicular polarization, where light is polarized perpendicular to the spinning axis. We can deconstruct this band into contributions from alpha helix and random coil.

IV. **Conclusion**

Using FTIR spectroscopy performed with polarized light in the mid-infrared range of 600 to 4000 cm^{-1}, we observed a number of vibrational modes in the silk of the recluse spider. We assign these modes to bending and stretching vibrations of various types of chemical bonds. We observe a certain degree of anisotropy in the infrared data. Additionally, we determined that the ß-sheet composition of the silk is about 26%. These results are consistent with similar measurements conducted using Raman spectroscopy.

References

[1] H.C. Schniepp, S.R. Koebley, and F. Vollrath, Adv. Mater. **25**, 7028 (2013).

[2] S. Keten, Z. Xu, B. Ihle, and M.J. Buehler, Nat. Mater. **9**, 359 (2010).

[3] S.R. Koebley, F. Vollrath, and H.C. Schniepp, Mater. Horiz. (2017).

[4] F.G. Omenetto and D.L. Kaplan, Science (80-.). **329**, 528 (2010).

[5] J.G. Hardy, L.M. R??mer, and T.R. Scheibel, Polymer (Guildf). **49**, 4309 (2008).

[6] D.-H. Kim, J. Viventi, J.J. Amsden, J. Xiao, L. Vigeland, Y.-S. Kim, J.A. Blanco, B. Panilaitis, E.S. Frechette, D. Contreras, D.L. Kaplan, F.G. Omenetto, Y. Huang, K.-C. Hwang, M.R. Zakin, B. Litt, and J.A. Rogers, Nat. Mater. **9**, 511 (2010).

[7] A. Sponner, W. Vater, and S. Monajembashi, PLoS One (2007).

[8] M.-E. Rousseau, T. Lefevre, L. Beaulieu, T. Asakura, and M. Pezolet, Biomacromolecules **5**, 2247 (2004).

[9] Y. Termonia, in *Struct. Biol. Mater.* (Pergamon Press, New York, 2000), pp. 337–349.

[10] Y. Termonia, Macromolecules **27**, 7378 (1994).

[11] A.J.D. Van Beek, S. Hess, F. Vollrath, B.H. Meier, J.D. Van Beek, S. Hesst, F. Vollrath, and B.H. Meier, PNAS **99**, 10266 (2016).

[12] A.H. Simmons, C.A. Michal, and L.W. Jelinskit, Am. Assoc. Adv. Sci. **271**, 84 (2016).

[13] M. Heim, L. Römer, T. Scheibel, L. Ro, and M. Heim, Chem. Soc. Rev. **39**, 156 (2010).

[14] T. Lefèvre, M.-E. Rousseau, and M. Pézolet, Biophys. J . **92**, 2885 (2007).

[15] S. Ling, Z. Qi, D.P. Knight, Z. Shao, and X. Chen, Biomacromolecules **12**, 3344 (2011).

[16] P. Papadopoulos, J. Sölter, and F. Kremer, Colloid Polym. Sci. **287**, 231 (2009).

[17] P. Papadopoulos, J. Sölter, and F. Kremer, Eur. Phys. J. E **24**, 193 (2007).

[18] P. Yu and M. Cardona, *Fundamentals of Semiconductors*, 3rd ed. (Springer, 2010).

[19] M. Dressel and G. Gruner, *Electrodynamics of Solids*, 1st ed. (Cambridge University Press, 2002).

[20] E.W. Weisstein, Eric Weisstein's World Sci. (2007).

[21] D. Wilson, R. Valluzzi, and D. Kaplan, Biophys. J. **78**, 617 (2000).

[22] M. Jackson and H.H. Mantsch, Crit. Rev. Biochem. Mol. Biol. **30**, 95 (1995).

[23]*Guide to Using WVASE2* (J. A. Woollam Co., Inc., 2010).

[24] S. Kubik, Angew. Chem. Int. Ed. **41**, 2721 (2002).

[25] B.L. Thiel, K.B. Guess, and C. Viney, Biopolymers **41**, 703 (1996).

[26] S. Keten and M.J. Buehler, J. R. Soc. Interface **7**, 1709 (2010).

[27] S. Keten and M.J. Buehler, Nano Lett. **8**, 743 (2008).

[28] S. Keten and M.J. Buehler, Phys. Rev. Lett. **100**, 1 (2008).

[29] B.L. Thiel, D.D. Kunkel, and C. Viney, Biopolymers **34**, 1089 (1994).

[30] W.H. Moore and S. Krimm, Biopolymers **15**, 2465 (1976).

[31] J.F. Rabolt, W.H. Moore, and S. Krimm, Macromolecules **10**, 1065 (1977).

[32] A. Dwivedi and S. Krimm, Macromolecules **15**, 186 (1982).

[33] S. Krimm and J. Bandekdar, Int. J. Pept. Protein Res. **19**, 1 (1980).

[34] W.H. Moore, S. Krimm, and H.M. Randall, Biopolymers **15**, 2465 (1976).

[35] J. Kong and S. Yu, Acta Biochim. Biophys. Sin. (Shanghai). **39**, 549 (2007).

[36] W.H. Moore and S. Krimm, Biopolymers **15**, 2439 (1976).

[37] A. Barth, Biochim. Biophys. Acta **1767**, 1073 (2007).

[38] K. Taga, M.G. Sowa, J. Wang, H. Etori, T. Yoshida, H. Okabayashi, and H.H. Mantsch, Vib. Spectrosc. **14**, 143 (1997).

[39] W. Gallagher, *FTIR Analysis of Protein Structure* (Eau Claire, WI, 1997).

[40] S.N. Timasheff and G.D. Fasman, *Structure and Stability of Biological Macromolecules* (Marcel Dekker, New York, 1969).

[41] S. Cai and B.R. Singh, Biophys. Chem. **80**, 7 (1999).

[42] F.N. Fu, D.B. DeOliveira, W.R. Trumble, H.K. Sarkar, and B.R. Singh, Appl. Spectrosc. **48**, 1432 (1994).

[43] A.D. Parkhe, S.K. Seeley, K. Gardner, L. Thompson, and R. V. Lewis, J. Mol. Recogn. **10**, 1 (1997).